ISSN 2616-5775 Vol. 8, Issue 10: 81-89, DOI: 10.25236/AJCIS.2025.081011

Implementation of Image Sensor Temperature Compensation Algorithm Based on FPGA

Liu Yang[1,2,a,*], Ziyang Zhang[1,b]

[1]School of Mechanical and Electrical Engineering, Hubei Polytechnic University, Huangshi, 435003, Hubei, China
[2]Hubei Key Laboratory of Intelligent Conveying Technology and Device, Hubei Polytechnic University, Huangshi, 435003, Hubei, China
[a]201113@hbpu.edu.cn, [b]wgdytc@163.com
[*]Corresponding author

Abstract: *The accuracy of sensors significantly affects system detection performance. However, environmental and experimental factors often cause deviations in sensor output. As key tools for obtaining external information, sensors require effective data processing to extract meaningful insights. This paper studies a temperature compensation algorithm for image sensors based on FPGA technology, which enhances processing efficiency and accuracy. Using an improved partial least squares method, irrelevant variables are removed through correlation analysis, and a polynomial relationship between correction coefficients and environmental parameters is established to achieve compensation. A multi-stage pipeline structure is adopted to leverage FPGA's parallel processing capability, improving algorithm speed. Experimental results show that the correction coefficient is 1.18 at 0 °C and 1.02 at 20 °C, indicating optimal sensor performance near 20 °C.*

Keywords: *Temperature Compensation Algorithm, Sensor Principle, FPGA Image, Data Compensation*

1. Introduction

In daily life, people need to transmit and process information frequently, and sensors are important tools for data collection and processing. With the continuous advancement of technology, data signals have become popular in the social field as a carrier of information. All sources of information need the help of sensors, but the output and input data of sensors are not completely linear, which will deviate from the actual situation. In order to reduce the error and improve its accuracy, in addition to the performance of the material itself, it can also compensate the signal. Therefore, it is necessary to combine the sensor with the temperature compensation algorithm.

Sensors are widely used as important tools for information acquisition. Kumar V.N. designed an intelligent pressure sensor based on ANN with a range of 0–100 psig. It uses an improved Schering bridge circuit and LM algorithm to achieve high accuracy and temperature compensation with an error of ±0.8% FS (10–35 °C) [1]. A.H.C. proposed a lithium battery hybrid estimation method, which combines state space observation and online parameter identification to improve stability [2]. Zhao C. combined Zernike moments with improved gradient Hough transform to achieve a center accuracy of 0.1 pixels and a radius of 0.05 pixels for circular hole detection. The detection speed and robustness are better than traditional algorithms [3]. Li X. used trapezoidal digital integral to compensate for cone error and double helix error, which significantly improved the navigation accuracy and dynamic performance of the SINS algorithm [4]. The above studies focus on the sensor compensation principle, but have not yet been combined with FPGA image processing.

As a programmable chip, FPGA plays an important role in image processing. Leon G. implemented noise estimation matrix calculation on FPGA based on orthogonal transformation, avoiding the numerical instability of LLS equation, and improved computational efficiency through modular QR decomposition [5]. Ambalathankandy P. implemented a real-time tone mapping algorithm based on exponential mapping on FPGA, combined local and global information to improve image brightness and contrast, and verified its excellent performance through high PSNR and SSIM [6]. Puglia L. proposed a stereo vision algorithm based on DNA sequence alignment, realized real-time image alignment on low-power FPGA, and has good portability [7]. Varshovi H. designed a wireless multimedia sensor network, used Spartan-6 FPGA to perform motion detection at the node end and upload time and location information to achieve efficient image monitoring [8]. However, these studies mostly focus on FPGA image processing and lack deep integration with sensors.

With the improvement of science and technology, the processing of daily information is also increasingly complex. According to the research, the actual value of the first test result of the traditional partial least squares regression is 5, and the test value is 5.5. The actual value of the second test result is 4, and the test value is 2.3. It can be seen that under the fitting of the traditional algorithm, there is a large deviation between the test value and the actual value. From the improved fitting results, the actual value of the first test result is 5, and the test value is 4.9. The actual value of the second test result is 4, and the test value is 3.8. Through two sets of test results, it is found that the improved algorithm is more suitable for nonlinear regression fitting and reduces the error very well.

2. FPGA Image Sensor Temperature Compensation Algorithm

Image processing technology appeared in the last century and has had a long development history. With the promotion of science and technology, its treatment effect is also improving [9-10]. In the process of image processing, a large number of image processing methods are used, but due to cost considerations, computer software is used for processing in most cases. However, with the continuous upgrading of user needs and the increase of image information data, image processing algorithms are also rising. This makes the image processing more difficult. If it still adopts the traditional image processing method, it will not only reduce the work efficiency, but also reduce the quality of image processing [11-12]. Figure 1 shows the computer software image processing structure:

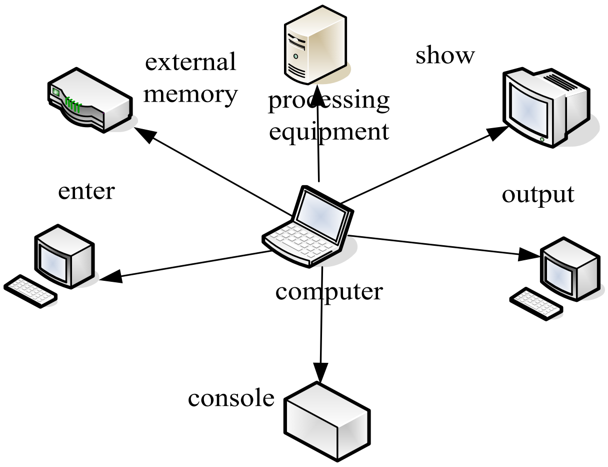

Figure 1 Computer software image processing structure

Because the computer is insufficient in software processing of images, more and more methods are adopted to implement it by hardware design [13]. With the rapid development of electronic technology, various digital hardware processors such as FPGA have appeared one after another. They are applied to various image processing systems to improve the quality and efficiency of image processing [14-15].

Due to insufficient resources of early FPGA chips, it cannot meet the requirements of large-scale applications. It is usually used as a co-processor of a digital signal processor (DSP) [16]. The FPGA is responsible for image acquisition, and the acquired image data is directly sent to the DSP for processing. Although this method can also process images, the processing speed needs to be improved. With the continuous progress of science and technology, the integration degree of FPGA is getting better and better, and its advantages in image processing are more and more obvious [17-18].

The existing image processing system traditionally includes computer projection image processing system and DSP embedded special image processing system [19]. Commonly used hardware parallel processing circuits in FPGA algorithms have two modes: pipeline and parallel array connection. The pipeline connection mode is to connect each processing module according to a certain rule [20]. Often experiments are performed in dividing a large task into several small tasks. Each small task has multiple sub-circuits connected in series, and each data enters the pipeline circuit in turn. In the parallel array connection mode, the input data can be divided into multiple parts and enter into independent circuits to carry out the calculation at the same time. In the process of image processing, parallel technology has become a method that can rapidly increase the speed of image processing. In the parallel processing mode, the algorithm is the core element, and the software and hardware are the tools for implementation. By taking advantage of FPGA hardware parallel data processing capabilities and multi-stage pipeline design advantages, it can process multiple data simultaneously. It completes image processing tasks quickly and efficiently.

With the advancement of global science and technology, the role of sensors in social production is becoming more and more important. At the same time, the production requirements are constantly upgraded, which also puts forward higher requirements for the performance of the sensor. As a tool for information transmission, the accuracy of the sensor is closely related to the operation of the machine. The quality of the sensor drive circuit design will affect the acquisition and transmission of real-time image data, which greatly affects the imaging effect of the image sensor.

In order to better compensate the dynamic characteristics of the sensor, it is first necessary to discuss the dynamic characteristics of the sensor. The sensor with better dynamic characteristics can monitor the signal change process of the target object in real time. There are many sensors in use, and their dynamic characteristics will greatly affect the measurement accuracy of the sensors, and the output of these sensors cannot completely and accurately reproduce the input signal.

Sensors can capture signals, which provide a way for people to perceive natural information. As a kind of test system, the exploration of the relevant characteristics of the sensor has always been the focus of research. Before using the sensor, we first need to understand its dynamic characteristics, and the results obtained in this inverse are closer to the real situation and improve its accuracy.

$$g_c \frac{p^c u}{pr^c} + \cdots + g_1 \frac{pu}{pr} + g_0 u = q_k \frac{p^k o}{pr^k} + \cdots + q_1 \frac{po}{pr} + q_0 o \tag{1}$$

In the above function expressions, g_c and q_k represent the relevant parameters of the system.

$$g_1 \frac{pu}{pr} + g_0 u = q_0 o \tag{2}$$

$$\frac{g_1}{g_0} \frac{pu}{pr} + u = \frac{q_0}{g_0} o \tag{3}$$

In the above expression, $\frac{g_1}{g_0}$ represents the time constant of the sensor, and $\frac{q_0}{g_0}$ represents the sensitivity of the sensor.

$$g_2 \frac{p^2 u}{pr^2} + g_1 \frac{pu}{pr} + g_0 u = q_0 o \tag{4}$$

Equation (4) represents a second-order system of differential equations.

$$\frac{2}{\mu_i^2} \frac{p^2 u}{pr^2} + \frac{3\delta}{\mu_i} \frac{pu}{pr} + u = yo \tag{5}$$

In the above function, μ_i is the frequency of the sensor, δ is the damping coefficient of the sensor, and y is its sensitivity.

$$\mathrm{u(c)} = \int \mathrm{u(\rho)\varepsilon(k-\rho)d\rho} \tag{6}$$

$$\mathrm{f(c)} = \int \mathrm{u(\rho)s(k-\rho)d\rho} \tag{7}$$

$$\mathrm{f(c)} = \int \mathrm{s(\rho)u(k-\rho)d\rho} \tag{8}$$

In the above function, $\mathrm{u(\rho)}$ represents the signal input of the system, and $\mathrm{f(c)}$ represents the signal output of the system.

$$\mathrm{s(k)} = \frac{2}{3\pi} \int \mathrm{L(q)\gamma^{qw}dq} \tag{9}$$

$$\mathrm{L(q)} = \int \mathrm{s(k)\gamma^{-qw}dk} \tag{10}$$

In equation (9) and equation (10), $\mathrm{s(k)}$ represents the unit impulse response, and $\mathrm{L(q)}$ represents the transfer function.

$$\mathrm{u(v)} + \sum \mathrm{p_r u(v-r)} = \sum \mathrm{e_o w(v-o)} \tag{11}$$

w represents the input and u represents the output.

$$\mathrm{u(v)} = -\sum \mathrm{p_r u(v-r)} + \sum \mathrm{e_o w(v-o)} + \mathrm{\tau(v)} \tag{12}$$

In the above function, $\tau(v)$ represents the measurement error.

In the actual test process, the actual output and the test output cannot be completely consistent, so dynamic errors are very common. But we need to reduce this error as much as possible in the measurement process, and get the signal with the highest possible progress.

$$g(z) = I_0 s(z - \sigma) \tag{13}$$

In the above function expression, both I_0 and σ are constants. At this time, the output of the sensor reproduces the measured signal, and the sensor represented by this equation is distortion-free.

$$U(\mu\vartheta) = \frac{R(\mu\vartheta)}{K(\mu\vartheta)} = I_0 \delta^{-\mu\vartheta} \tag{14}$$

$U(\mu\vartheta)$ represents the frequency response characteristic.

$$|U(\mu\vartheta)| = I_0 \tag{15}$$

$$\rho(\mu\vartheta) = -\vartheta\beta \tag{16}$$

The equation (15) represents the frequency-amplitude characteristic, and the equation (16) represents the phase-frequency characteristic.

$$\alpha(z) = G\left[\left(U(\mu\vartheta) - U_a(\mu\vartheta)\right)T(\mu\vartheta)\right] \tag{17}$$

In the above function, $U_a(\mu\vartheta)$ represents the actual sensor frequency characteristic, and $\alpha(z)$ represents the sensor system error.

3. Implementation Experiment of Sensor Temperature Compensation Algorithm

Partial least squares regression plays a very important role in solving linear regression problems. However, most of the problems that need to be solved in real life are nonlinear, so if the traditional partial least squares regression algorithm is used, the error is very large. Therefore, it is necessary to perform data compensation on the original basis.

Traditional least squares regression fails to fit correctly mainly because of the presence of nonlinear terms in the data. Therefore, how to deal with higher-order terms becomes an important step in the successful use of partial least squares regression.

$$p = q + c_1 a + c_2 a^2 + \mu \tag{18}$$

Equation (18) is a typical nonlinear equation, and when we process its higher-order terms, we can get:

$$p = q + c_1 a + c_2 h + \mu \tag{19}$$

In the above equation, $a^2 = h$. With this improvement, the original nonlinear fit can be transformed into a linear model.

According to the above situation, when fitting the first-order polynomial, the error has been controlled. At this time, there is no need to iteratively reduce the error, so we can regard the traditional partial least squares regression as a special case of the improved partial least squares regression. In order to test the effect of the improved partial least squares regression, we compared it with the traditional fitting method. The details are as follows:

Table 1 Test data specifics

Projects	1	2	3	4	5	6
a	1	2	3	4	5	6
p	1	0	2	0	4	0
t	2	5	7	6	23	8

According to the data in Table 1, we used 6 sets of data for testing. During the test, the two groups of data are the same, which avoids the interference of different data on the test situation. According to the above linear fitting function, t represents the dependent variable, while a and p represent the independent variables. According to the test data provided, we calculated the traditional partial least squares regression and the improved partial least squares regression separately and found:

The traditional partial least squares regression fitting situation is:

$$t = -1.9 + 1.6a + 4.7p \tag{20}$$

The improved partial least squares regression fitting situation is:

$$t = 0.6 + 1.1a + 1.5p + 0.4p^2 + 0.3ap \tag{21}$$

According to the two sets of fitting conditions, the improved algorithm can reduce the fitting error by continuously optimizing the higher-order terms. Essentially, this step is an iterative process. Depending on the error situation, it can be fitted to different types of multinomial modes. Through the improvement in this way, its error has been better controlled.

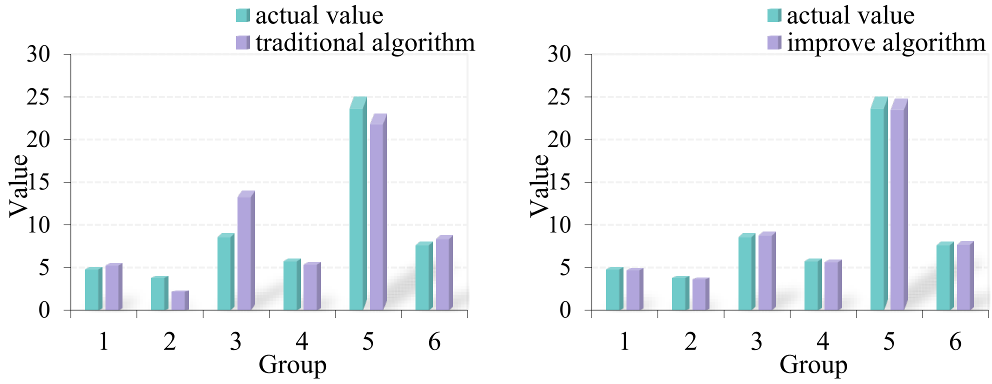

Figure 2 Comparative analysis of test results under different algorithms

According to the data in Figure 2, we tested the above data using different fitting methods. First of all, from the results of traditional partial least squares regression, we conducted a total of 6 tests. According to the experimental data, it is found that the actual value of the first test result is 5, and the test value is 5.5. The actual value of the second test result is 4, and the test value is 2.3; the third test result is the actual value of 9, and the test value is 14. The actual value of the fourth test result is 6, and the test value is 5.6; the fifth test result is the actual value of 25, and the test value is 23. The actual value of the sixth test result is 8, and the test value is 8.8. According to the data, under the fitting of the traditional algorithm, there is a large deviation between the test value and the actual value.

From the improved partial least squares regression fitting results, the actual value of the first test result is 5, and the test value is 4.9. The actual value of the second test result is 4, and the test value is 3.8; the third test result is the actual value of 9, and the test value is 9.2. The actual value of the fourth test result is 6, and the test value is 5.9; the fifth test result is 25, and the test value is 24.8; the sixth test result is 8, and the test value is 8.1. According to the data, under the improved algorithm, the fitting effect of the data has been greatly improved. Through two sets of test results, it is found that the improved algorithm is more suitable for nonlinear regression fitting and reduces the error very well.

FPGA is developed on the basis of programmable devices. With the maturity of development technology, FPGA can not only solve the shortcomings of the circuit, but also solve the problem of insufficient number of gate circuits in programmable devices. Because of its structural and development advantages, FPGAs are used in many fields.

When the sensor data is retrieved from the database, data compensation for each part of the gas sensor is required. During execution, it is necessary to select environmental factors that may affect the accuracy of the sensor value, and train the sample data according to the corresponding factors. It fits the sensor correction factor and environmental parameters, and uses this relationship as a parameter when compensating the sensor in the system. Another parameter during compensation is the measured value of the current state of the sensor. In the experiment, we take carbon monoxide in the standard volume fraction as an example, the specific situation is as follows:

*Table 2 Measurements of the sensor when carbon monoxide is 200*10-6 ppm*

Sample	1	2	3	4	5	6
Temperature (°C)	0	10	20	30	40	50
Humidity (%)	40	40	40	40	40	40
Measured value (10-6 ppm)	161	172	189	205	211	220

According to the data in Table 2, this test of the sensor controls the experimental conditions. According to the specific situation, when the temperature is 0°C and the humidity is 40%, the measured value is 161*10-6 ppm. When the temperature is 10°C and the humidity is 40%, its measured value is 172*10-6 ppm. When the temperature is 20°C and the humidity is 40%, its measured value is 189*10-6 ppm. When the temperature is 30°C and the humidity is 40%, its measured value is 205*10-6 ppm. When the temperature is 40°C and the humidity is 40%, its measured value is 211*10-6 ppm. When the temperature is 50°C and the humidity is 40%, its measured value is 220*10-6 ppm. According to this data, the humidity remains consistent, and as the temperature increases, so does its measurement. If the difference between the measured value and the actual value is large, the regression model needs to be iterated, and the higher-order term is used as a new variable to reduce the error.

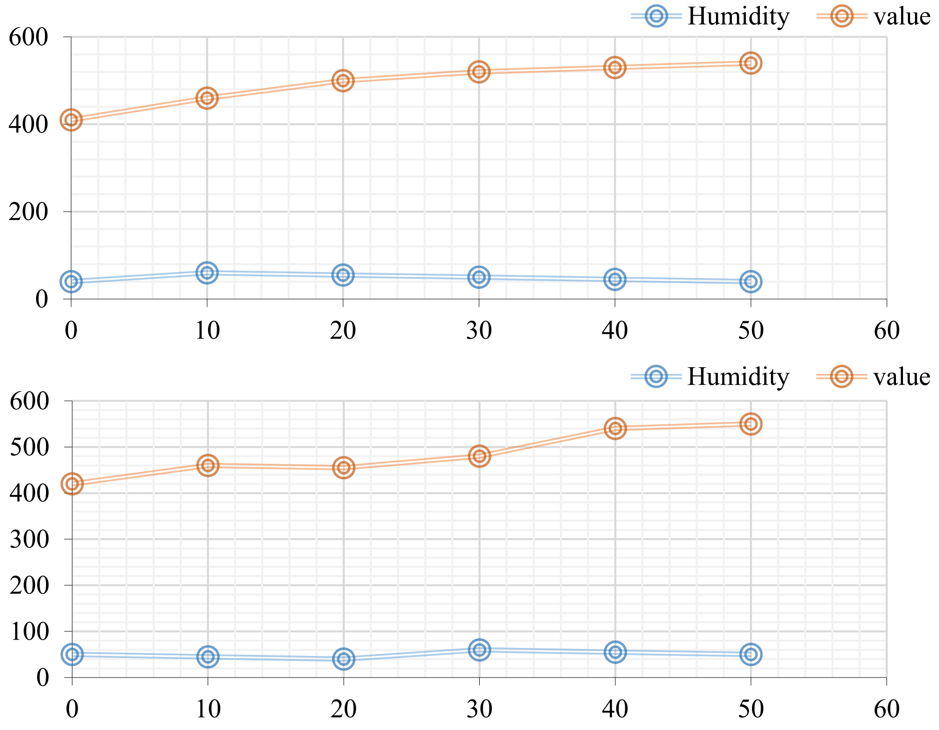

*Figure 3 The measured values of the sensor in different environments when the carbon monoxide is 500*10-6 ppm*

According to the data in Figure 3, we have carried out a comparative analysis of the sensor measurement values under different temperatures and humidity. According to the analysis, in the overall environment system, when the temperature is 0, the sensor measurement value is 410*10-6 ppm when the humidity is 40%, and the sensor measurement value is 420*10-6 ppm when the humidity is 50%. When the temperature is 10, the sensor measurement value is 460*10-6 ppm when the humidity is 60%, and the sensor measurement value is 460*10-6 ppm when the humidity is 40%. When the temperature is 20, the sensor measurement value is 500*10-6 ppm when the humidity is 55%, and the sensor measurement value is 455*10-6 ppm when the humidity is 40%. When the temperature is 30, the sensor measurement value is 520*10-6 ppm when the humidity is 50%, and the sensor measurement value is 480*10-6 ppm when the humidity is 60%. When the temperature is 40, the sensor measurement value is 530*10-6 ppm when the humidity is 45%, and the sensor measurement value is 540*10-6 ppm when the humidity is 55%. When the temperature is 50, the sensor measurement value is 540*10-6 ppm when the humidity is 40%, and the sensor measurement value is 550*10-6 ppm when the humidity is 50%. According to this data, under the same conditions, the higher the humidity, the higher the sensor measurement value. And according to the experimental data, it can be known that the more iterations in the system, the more accurate the measured value.

4. Temperature Compensation Algorithm

Although there are all kinds of data around us, the data around us is not completely usable directly, at least there are very few data that can be directly used. In most cases, the collected information needs to be converted, and the information we can directly use in the end is converted from electrical signals. The sensor plays an important role in this process, but the sensor does not really reflect the measurand, so the relevant data needs to be compensated.

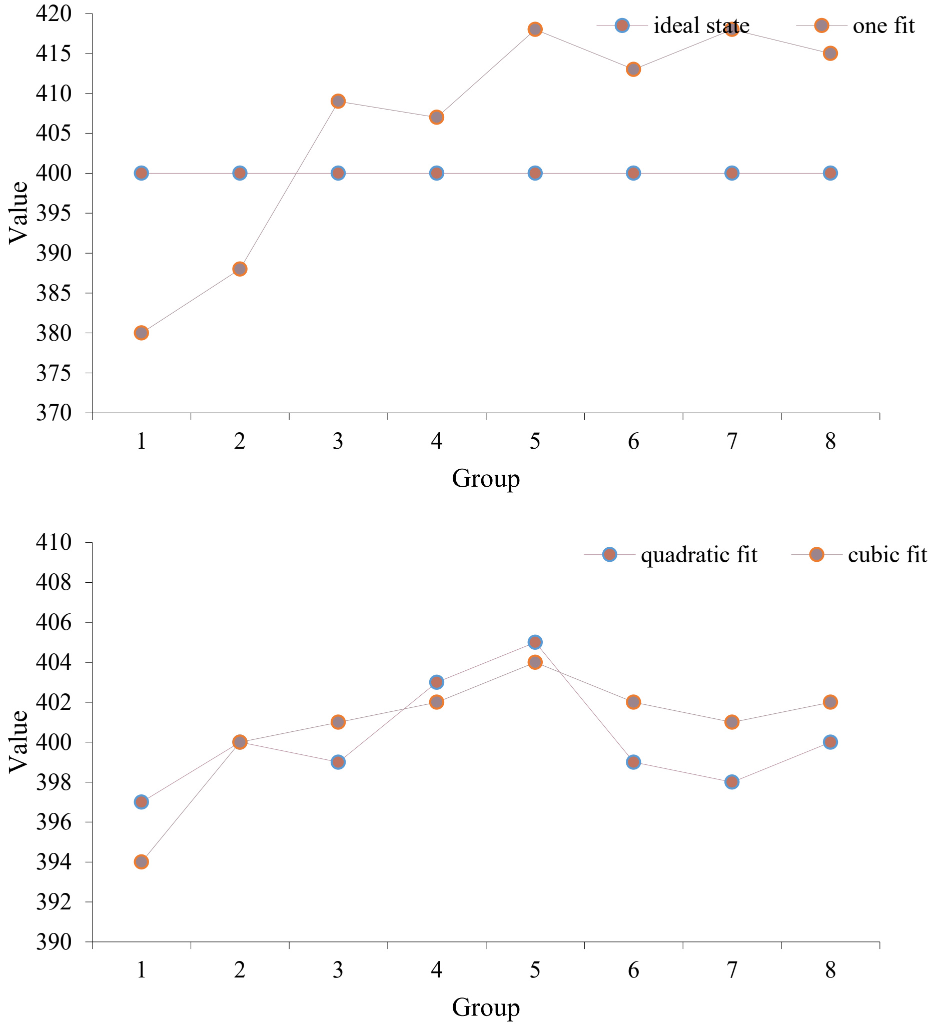

Figure 4 Comparative analysis of different fitting results

According to the data in Figure 4, in order to check the actual compensation effect of different algorithms, we have analyzed the test situations under different fitting conditions. In this comparison, we conducted 8 tests. First, we analyze the ideal situation. According to the data in the ideal state, in this case, the compensated data are all 400*10-6 ppm, and the situation is very stable. In one term fitting, the first test value is 380*10-6 ppm; the second test value is 388*10-6 ppm. The third test value was 409*10-6 ppm. The fourth test value is 407*10-6 ppm; the fifth test value is 418*10-6 ppm. The sixth test value was 413*10-6 ppm. The seventh test value is 418*10-6 ppm; the eighth test value is 415*10-6 ppm. According to the fitting situation of the first-order term, it can be known that in this case, the magnitude of the value change after compensation is very large. Although the compensation value tends to be stable as the number of iterations increases, it deviates greatly from the numerical value in the ideal state. Compared with the actual information, the output has a large error.

From the fitting situation of the quadratic term and the cubic term, the variation of the fitted data of the two groups is very small compared with the fitted data of the primary term. And from the perspective of the cubic term fitting, the compensated value is very close to the ideal value, and the accuracy has been greatly improved. According to the above analysis, it can be inferred that the polynomial regression will be infinitely close to the actual curve with the increase of high-order terms. It can continuously approach the ideal state.

According to the data in Figure 5, we have explored the compensation value and measurement value of the sensor when the temperature and humidity are kept constant. According to the actual situation, when the measurement value is 0*10-6 ppm, the compensation value is 2*10-6 ppm; when the measurement value is 100*10-6 ppm, the compensation value is 95*10-6 ppm. When the measured value is 200*10-6 ppm, its compensation value is 195*10-6 ppm; when the measured value is 300*10-6 ppm, its compensation value is 294*10-6 ppm. When the measured value is 400*10-6 ppm, its compensation value is 390*10-6 ppm; when the measured value is 500*10-6 ppm, its compensation value is 586*10-6 ppm. From this data, it can be seen that the compensation value and the measured value are upward sloping lines. In an ideal state, the correction coefficient is constant and the slope is the same. Therefore, in the actual measurement situation, the sensor measurement value can be quickly compensated according to the actual situation, so that the error between it and the actual result is smaller.

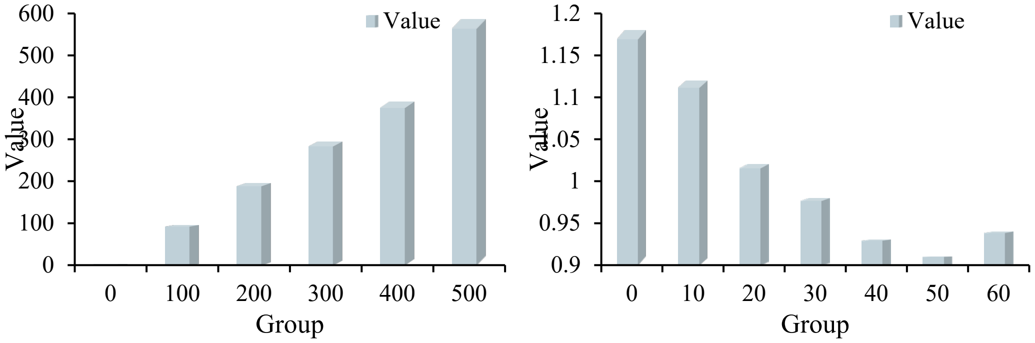

Figure 5 Analysis of temperature compensation values under different conditions

In order to explore the variation of the correction factor, we investigate it when the single variables of temperature and humidity are constant. According to the actual situation, when the temperature is 0 °C, the correction coefficient is 1.18. When the temperature is 10°C, the correction factor is 1.12; when the temperature is 20°C, the correction factor is 1.02; when the temperature is 30°C, the correction factor is 0.98. When the temperature is 40°C, the correction factor is 0.93; when the temperature is 50°C, the correction factor is 0.91. When the temperature is 60°C, the correction factor is 0.94. From this situation, it can be seen that the correction coefficient is highest when the temperature is 0°C, and then decreases as the temperature increases. When its temperature reaches 50°C, the correction coefficient is the lowest, and then the correction coefficient increases slowly with the increase of temperature. It can be seen that at 0°C, the difference before and after the sensor compensation is the largest, so we can think that its measurement effect at 0°C is the worst. When the temperature is 20°C, the correction coefficient is the closest to 1, indicating that the difference between before and after compensation is very small. It shows that the sensor works best at this time.

5. Conclusion

With the support of science and technology, the life around us is closely related to data and information. Image processing technology is currently used in many fields, and it is usually processed by computer software at first. However, with the upgrade of actual requirements, traditional processing methods are no longer applicable. The emergence of FPGA technology provides a new idea for image processing. The collection of continuous and data information or image information requires the use of sensors, but the sensors will be disturbed by the outside world during the collection process, resulting in the deviation of the collected information from the actual situation. The purpose of this paper is to study the research and implementation of temperature compensation algorithm for image sensor based on FPGA. The information is collected through sensors, which is then processed using FPGA technology to derive its deviation from the actual results. In the process of processing, this paper compensates the relevant data to reduce the processing error. According to the research findings, the error can be effectively controlled by the improved partial least squares regression fitting method. Although this paper draws some conclusions, there are still shortcomings. The article takes limited FPGA resources. It only uses acquisition and preprocessing, and it is expected that the entire system can be applied in future research.

Acknowledgements

This work was supported by Talent Introduction Project of Hubei Polytechnic University (22xjz27R), Hubei Key Laboratory of intelligent transportation technology and device, Hubei Polytechnic University (2024XM103), Teaching and Research Project of Hubei Polytechnic University (2024C12), Project of Hubei Province College Students' Innovation and Entrepreneurship Training Program (202410920025).

References

[1] Kumar V N, Narayana K. DEVELOPMENT OF AN INTELLIGENT PRESSURE SENSOR WITH TEMPERATURE COMPENSATION[J]. Journal of Engineering Science and Technology, 2017, 12(7): 1723-1739.

[2] A H C, B H G. Online parameter and state estimation of lithium-ion batteries under temperature effects[J]. Electric Power Systems Research, 2017, 145(Apr.):73-82.

[3] Zhao C, H Ding, Cao G. A New Method for Detecting Compensation Hole Parameters of Automobile Brake Master Cylinder Based on Machine Vision[J]. Journal of Advanced Transportation, 2021, 2021(3):1-14.

[4] Li X, Xiong Z, Liu J Y. Improved Coning and Sculling Error Compensation Algorithms Based on Dual Quaternion for Strapdown Inertial Navigation System[J]. Acta Armamentarii, 2017, 38(7): 1336-1347.

[5] Leon G, Gonzalez C, Mayo R. Noise estimation for hyperspectral subspace identification on FPGAs[J]. Journal of Supercomputing, 2019, 75(3):1323-1335.

[6] Ambalathankandy P, Hore A, Yadid-Pecht O. An FPGA implementation of a tone mapping algorithm with a halo-reducing filter[J]. Journal of Real-Time Image Processing, 2019, 16(4): 1317-1333.

[7] Puglia L, Vigliar M, Raiconi G. Real-Time Low-Power FPGA Architecture for Stereo Vision[J]. IEEE Transactions on Circuits and Systems II: Express Briefs, 2017, 64(11):1307-1311.

[8] Varshovi H, Kavian Y S, Ansari-Asl K. Design and implementing wireless multimedia sensor network for movement detection using FPGA local co-processing[J]. Multimedia Tools and Applications, 2019, 78(13):17413-17435.

[9] Pathak K, Bansal M. A FPGA based Steganographic System Implementing a Modern Steganalysis Resistant LSB Algorithm[J]. Defence Science Journal, 2017, 67(5):551-558.

[10] Al-Mahmood A, Opoku M. A Study of FPGA-based System-on-Chip Designs for Real-Time Industrial Application[J]. International Journal of Computer Applications, 2017, 163(6):9-19.

[11] Perez-Patricio M, Aguilar-Gonzalez A. An FPGA-based smart camera for accurate chlorophyll estimations[J]. International journal of circuit theory and applications, 2018, 46(9):1663-1674.

[12] GF Araujo, R D'Amore, Fernandes D. Cost-sensitive FPGA implementation of SAR range-doppler algorithm[J]. IEEE Aerospace and Electronic Systems Magazine, 2018, 33(9):54-68.

[13] Lim J H, Ryu J Y. Edge Detection Control of Color Images Using FPGA[J]. Journal of Institute of Control, 2019, 25(10):936-941.

[14] Zhong L, Wang X, Lu S K. Implementation System of Human Eye Tracking Algorithm Based on FPGA[J]. Computers, Materials and Continua, 2019, 58(3):653-664.

[15] Réda, Yahiaoui, Farid. Parallelization of Fuzzy ARTMAP Architecture on FPGA: Multispectral Classification of ALSAT-2A Images[J]. IEEE Transactions on Industrial Electronics, 2017, 64(12): 9487-9495.

[16] Shadrin G K, Alontseva D L, Kussaiyn-Murat A T. Application of Compensation Algorithms to Control the Movement of a Robot Manipulator[J]. Acta Polytechnica Hungarica, 2020, 17(1):191-214.

[17] Luca A D, Sall F S, Khoury A. Leak Compensation Algorithms: The Key Remedy to Noninvasive Ventilation Failure[J]. Respiratory Care, 2017, 62(1):135-136.

[18] Xu L, Chen G, Li G. Model Predictive Control Based on Parametric Disturbance Compensation[J]. Mathematical Problems in Engineering, 2020, 2020(5):1-13.

[19] Wu S W, Zhou X G, Cao G M. The improvement on constitutive modeling of Nb-Ti micro alloyed steel by using intelligent algorithms[J]. Materials & Design, 2017, 116(feb.):676-685.

[20] Matyunin, Sergey A. Research on Characteristics of Fiber Optic Sensors for Anthropomorphous Robots [J]. Procedia Engineering, 2017, 176(Complete):128-136.